Optimal collinear Gaussian beams for spontaneous parametric down-conversion

Ryan S. Bennink[*]

Oak Ridge National Laboratory, Oak Ridge, Tennessee 37831, USA

I investigate the properties of spontaneous parametric down-conversion (SPDC) involving collinear Gaussian spatial modes for the pump and the photon collection optics. Approximate analytical and numerical results are obtained for the peak spectral density, photon bandwidth, pair collection probability, heralding ratio, and spectral purity as a function of crystal length and beam-focusing parameters. I address the optimization of these properties individually as well as jointly, and find focusing conditions that simultaneously bring the pair collection probability, heralding ratio, and spectral purity to near-optimal values. These properties are also found to be nearly scale invariant, that is, ultimately independent of crystal length. The results obtained here are expected to be useful for designing SPDC sources with high performance in multiple categories for the next generation of SPDC applications.

I. INTRODUCTION

Spontaneous parametric down-conversion (SPDC) is a process widely used to produce both entangled photon pairs and heralded single photons. SPDC photon sources play a key role in quantum cryptography, optical quantum computing, quantum metrology, and in fundamental studies of quantum mechanics. In many applications, a nonlinear optical crystal is pumped by a focused laser beam and the emitted SPDC light is collected into a pair of optical waveguides, such as an integrated optical circuit [1] or a fiber network [2]. Efforts over the past decade have led to some very bright SPDC sources [3,4]. As brightness has improved, interest has progressed from simply making SPDC sources brighter to controlling other properties of the emitted photons, such as the spectral entanglement in each photon pair [5–8]. While several papers in recent years [9–16] have addressed the question of how to focus the pump and/or collection optics optimally, some important questions remain. Since different studies have invoked slightly different assumptions and optimized slightly different measures, it is not clear how pump and/or collection focusing simultaneously affects all the quantities that are generally of interest, and what trade-offs (if any) exist between these quantities. Furthermore, the scaling laws for the optimized quantities and optimal parameter values are not readily apparent (e.g., whether it is possible to halve the crystal length and, through a change of beam parameters, obtain similar performance).

To address such questions, I present here a study of SPDC for the case in which the pump and collecting optics define collinear Gaussian spatial modes. While the theory is general, the envisioned context is SPDC in a periodically poled nonlinear crystal with emission in the visible or telecommunication spectral range (a common and useful configuration). In this study I consider five properties of the collected biphoton state that are commonly of interest: the joint spectral density, the photon bandwidths, the pair collection probability, the heralding ratio (photon pair to single photon collection ratio), and the spectral entanglement. These

properties are calculated—in some cases analytically, in some cases numerically—as functions of experimental parameters, yielding predictions for the absolute values of the properties as well as for the parameter values that optimize each property. Additionally, this study reveals several scaling laws and shows that some properties can be jointly optimized while others require a trade-off. Of the many results presented here, a few appear to differ from the predictions of others.

The paper is organized as follows: Section II establishes the foundational equations describing Gaussian optical modes and the quantum physics of SPDC. Sections III–VII derive expressions for the five properties mentioned above and discuss their dependence on experimental parameters. Section VIII discusses the results of this study in light of prior works, and Sec. IX summarizes the main conclusions.

II. SPDC WITH GAUSSIAN SPATIAL MODES

SPDC is the lowest-order effect of parametric interaction between a strong pump (p) field and two other fields, designated as signal (s) and idler (i), initially in the vacuum state. The quantum Hamiltonian governing this interaction is

$$\hat{H} = \int \varepsilon_0 (\boldsymbol{\chi}^{(2)}(\mathbf{r}) : \hat{\mathbf{E}}^+(\mathbf{r},t)\hat{\mathbf{E}}^-(\mathbf{r},t)\hat{\mathbf{E}}^-(\mathbf{r},t) + \text{H.c.}) d^3\mathbf{r}, \tag{1}$$

where $\mathbf{r} = (x,y,z)$ is the spatial coordinate, t is time, $\boldsymbol{\chi}^{(2)}(\mathbf{r})$ is the nonlinear susceptibility tensor, and $\hat{\mathbf{E}}^+(\mathbf{r},t) = \hat{\mathbf{E}}^-(\mathbf{r},t)^\dagger$ is the positive-frequency part of the electric-field quantum operator. In canonical treatments, the field is expanded in terms of an orthonormal set of modes. Since the interest here is in SPDC involving Gaussian spatial modes, I choose a modal expansion containing a Gaussian mode for each frequency ω. It will be sufficient to consider just these Gaussian modes until Sec. VII. In this case $\hat{\mathbf{E}}^+(\mathbf{r},t)$ may be written as

$$\hat{\mathbf{E}}^+(\mathbf{r},t) = \int_0^\infty d\omega \sqrt{\frac{\hbar\omega}{2\varepsilon_0}} \mathbf{E}_\omega(\mathbf{r}) e^{-i\omega t} \hat{a}_\omega(t) + \text{irrelevant}$$

non-Gaussian modes, $\tag{2}$

---
[*]benninkrs@ornl.gov

where $\mathbf{E}_\omega(\mathbf{r})$ is the electric-field function for the (Gaussian) mode of frequency ω and $\hat{a}_\omega^\dagger(t)$ is the operator that creates a photon in that mode.

The state resulting from the interaction (1) is obtained by applying the operator $\exp[-\frac{i}{\hbar}\int_{-\infty}^{\infty} dt\, \hat{H}(t)]$ to the initial state. The part of the state corresponding to SPDC, that is, the creation of a single pair of photons, is just the first-order term:

$$|\Psi_{\text{SPDC}}\rangle = -\frac{i}{\hbar}\int_{-\infty}^{\infty} dt\, \hat{H}(t)\,|\text{initial}\rangle. \quad (3)$$

The insertion of Eqs. (1) and (2) into (3) gives

$$|\Psi_{\text{SPDC}}\rangle = -i\int_0^\infty d\omega_s d\omega_i\, \psi(\omega_s,\omega_i)\hat{a}_{\omega_s}^\dagger \hat{a}_{\omega_i}^\dagger|\text{vac}\rangle, \quad (4)$$

where $|\text{vac}\rangle$ is the vacuum state of the signal and idler and

$$\psi(\omega_s,\omega_i) = \sqrt{\frac{2\pi^2\hbar N_p}{\varepsilon_0\lambda_p\lambda_s\lambda_i}}s(\omega_p)\mathcal{O}(\omega_s,\omega_i) \quad (5)$$

is the SPDC amplitude. Here ε_0 is the vacuum permittivity, $\lambda_j = 2\pi c/\omega_j$ is the free-space wavelength of field j ($j =$ p,s,i), and $\omega_p = \omega_s + \omega_i$. The pump field has been assumed to be in a coherent state with independent spectral and spatial dependence. Accordingly, the operator $\hat{a}_{\omega_p}$ has been replaced by the complex amplitude $a(\omega_p) = s(\omega_p)\sqrt{N_p}$, where $s(\omega_p)$ is the pump spectral amplitude [with $\int|s(\omega)|^2\, d\omega = 1$] and N_p is the mean number of pump photons (the pump energy divided by $\hbar\omega_p$). The quantity

$$\mathcal{O}(\omega_s,\omega_i) \equiv \int_{\text{medium}} \boldsymbol{\chi}^{(2)}(\mathbf{r}) : \mathbf{E}_{\omega_p}(\mathbf{r})\mathbf{E}_{\omega_s}^*(\mathbf{r})\mathbf{E}_{\omega_s}^*(\mathbf{r})\, d^3\mathbf{r} \quad (6)$$

is the spatial overlap of the pump, signal, and idler modes in the medium, which generalizes the sinc phase-matching function encountered in plane-wave treatments of SPDC [17]. The medium is taken to be a bulk material of length L centered at the origin, with a cross section large enough to contain the mode functions. The material may be ferroelectrically poled so that $\boldsymbol{\chi}^{(2)}(\mathbf{r})$ alternates sign with spatial period Λ.

The properties of the SPDC state can be calculated once particular forms are chosen for the pump spectrum $s(\omega_p)$ and the mode functions $\mathbf{E}_{\omega_j}(\mathbf{r})$. Consideration will be restricted to modes of the form

$$\mathbf{E}(\mathbf{r}) = \frac{\mathbf{e}}{\sqrt{\pi/2}}\frac{w}{q}\exp\left(-\frac{x^2+y^2}{q} + ikz\right), \quad (7)$$

which describes a linearly polarized, paraxial Gaussian beam with waist at the origin, propagating along the z axis in an optically uniform medium. Here w is the waist size, $\mathbf{e}$ is the polarization unit vector, $k = 2\pi n\omega/c$ is the wavenumber, n is the refractive index, and $q = w^2 + 2iz/k$. This choice is in part motivated by the fact that some of the best SPDC sources in existence involve Gaussian beams copropagating along one of the principle refractive axes of a transparent crystalline material, such as potassium titanyl phosphate or lithium niobate. (The anisotropy of the refractive index may be safely ignored in such cases.) Additionally, symmetry indicates that the spatial overlap is largest when the modes copropagate and have their waists colocated at the center of the crystal. This leaves the waist sizes w_p, w_s, w_i as the free parameters for mode optimization.

Using modes of the form (7), the mode overlap (6) is

$$\mathcal{O} = \frac{\sqrt{\epsilon}\chi_{\text{eff}}^{(2)}}{(\pi/2)^{3/2}}\int\frac{w_p w_s w_i}{q_p q_s^* q_i^*}\exp\left[-(x^2+y^2)\left(\frac{1}{q_p} + \frac{1}{q_s^*} + \frac{1}{q_i^*}\right)\right. $$
$$\left. + i(\Delta k + mK)z\right]dx\,dy\,dz. \quad (8)$$

Here $\Delta k = k_p - k_s - k_i$ is the wavenumber mismatch, $K = 2\pi/\Lambda$ is the poling spatial frequency, m is the order of quasi-phase-matching, $\chi_{\text{eff}}^{(2)} \equiv \boldsymbol{\chi}^{(2)} : \mathbf{e}_p\mathbf{e}_s\mathbf{e}_i$ is the effective nonlinear coefficient, and ϵ is an efficiency factor that includes Fresnel loss and the Fourier coefficient of the mth harmonic of the poling spatial function. Integrating over x and y yields

$$\mathcal{O} = \sqrt{\frac{8\epsilon}{\pi}}\chi_{\text{eff}}^{(2)}w_p w_s w_i\int_{-L/2}^{L/2}\frac{\exp[i(\Delta k + mK)z]}{q_s^* q_i^* + q_p q_i^* + q_p q_s^*}\,dz. \quad (9)$$

Before proceeding, it will be convenient to rewrite (9) in terms of dimensionless quantities. The primary independent variables are the phase mismatch

$$\Phi \equiv (\Delta k + mK)L \quad (10)$$

and the focal parameters

$$\xi_j \equiv \frac{L}{k_j w_j^2}, \quad (11)$$

where $\xi_j \gg 1$ ($\ll 1$) means that field j ($j =$ p,s,i) is focused strongly (weakly) relative to the length of the crystal.

I also define the auxiliary quantities

$$A_\pm \equiv 1 + \frac{k_s}{k_p}\frac{\xi_s}{\xi_p} \pm \frac{k_i}{k_p}\frac{\xi_i}{\xi_p}, \quad (12)$$

$$B_\pm \equiv \left(1 - \frac{\Delta k}{k_p}\right)\left(1 + \frac{k_s + \Delta k}{k_p - \Delta k}\frac{\xi_p}{\xi_s} \pm \frac{k_i + \Delta k}{k_p - \Delta k}\frac{\xi_p}{\xi_i}\right), \quad (13)$$

$$C \equiv \frac{\Delta k}{k_p}\frac{\xi_p^2}{\xi_s\xi_i}\frac{A_+}{B_+^2}, \quad (14)$$

and the aggregate focal parameter

$$\xi \equiv \frac{B_+}{A_+}\frac{\xi_s\xi_i}{\xi_p}. \quad (15)$$

The quantities A_+, B_+, and ξ are independent and uniquely determine ξ_s, ξ_i, and ξ_p. C is determined by A_+ and B_+. Note that $A_\pm$, $B_\pm$, and C do not depend on the absolute values of the focal parameters, but on the focus of the signal and idler *relative* to the pump. In terms of these dimensionless quantities, Eq. (5) may be written as

$$\psi(\omega_s,\omega_i) = \sqrt{\frac{8\pi^2\epsilon\hbar n_s n_i N_p L}{\varepsilon_0 n_p}}\frac{\chi_{\text{eff}}^{(2)}}{\lambda_s\lambda_i}\frac{s(\omega_p)}{\sqrt{A_+ B_+}}$$
$$\times \int_{-1}^{1}\frac{\sqrt{\xi}\exp(i\Phi l/2)}{1 - i\xi l - C\xi^2 l^2}\,dl. \quad (16)$$

Equation (16) will be the starting point for analysis in Secs. III–VI.

Four approximations will be invoked throughout this work in order to simplify analysis and yield more useful results. These approximations are reasonable for typical bulk SPDC sources, which may be defined as having the following characteristics: the length of the medium is $\gtrsim 1$ mm and its

refractive index is $\gtrsim 1.5$, the parametric interaction is quasi-phase-matched with a first-order grating of period $\Lambda \gtrsim 5\,\mu$m, and emission is in the visible or telecommunication spectral range, with $\lambda_s \lesssim 1.6\,\mu$m and $\lambda_p \lesssim 0.8\,\mu$m. When assessing the accuracy of approximate formulas, these values will be considered as representing the worst typical case. I will also consider a "reference source" consisting of degenerate type-II SPDC in 10-mm periodically poled potassium titanyl phosphate (PPKTP) with a 750-nm pump. This is similar to several sources that have been demonstrated to have good performance [3,4,18].

One approximation that will be used liberally is

$$1 \pm \frac{\Delta k}{k_j} \approx 1. \tag{17}$$

This approximation is motivated by the fact that efficient SPDC occurs when $\Delta k \approx -mK$, where mK/k_j is typically much smaller than 1.

Another approximation that will prove convenient is

$$C \approx 0. \tag{18}$$

The actual value of C depends in a complicated way upon the experimental parameters, but can be shown to obey the bound

$$|C| \leqslant \frac{|\Delta k|k_p}{4k_s k_i} = \left| \frac{\Phi k_p}{4k_s k_i L} - \frac{mK k_p}{4k_s k_i} \right| \tag{19}$$

when (17) is valid. One then has $|C| \lesssim 0.1$ near-phase-matching conditions, which turns out to be small enough to make (18) a fair approximation over the range of focusing that is desirable with respect to the five properties of the state considered here.

The third approximation is that the frequency dependence of (16) is determined essentially by the pump spectrum $s(\omega_p)$ and the frequency dependence of the wave mismatch Δk. That is, I take

$$A_\pm, B_\pm, \xi_j, \sqrt{\frac{\epsilon n_s n_i}{n_p}}\frac{\chi_{\text{eff}}^{(2)}}{\lambda_s \lambda_i} \approx \text{const} \tag{20}$$

over the range of (ω_s, ω_i) for which the amplitude is appreciable. For (20) to hold, the bandwidths of the photons must be much smaller than an optical frequency. Type-II and nondegenerate type-I SPDC sources typically satisfy this condition, but frequency-degenerate type-I sources and sources made of very short crystals, which tend to have large bandwidths, may not.

Finally, after Sec. III it will be assumed the wave mismatch Δk has a predominantly linear frequency dependence,

$$\delta k_j \approx \frac{n_j'}{c}\delta \omega_j, \tag{21}$$

where $n_j' \equiv c\,\partial k_j/\partial \omega$ is the group index of mode j and $\delta \omega_j$ (δk_j) denotes a shift from the nominal frequency (wavenumber) of mode j. Again, this approximation is generally valid for type-II and nondegenerate type-I SPDC sources, but not for frequency-degenerate type-I sources.

The impact of these approximations, particularly (18), will be addressed more fully in the context of each major result.

III. JOINT SPECTRAL DENSITY

The joint spectral density $|\psi(\omega_s,\omega_i)|^2$ is the expected number of photon pairs, per signal bandwidth per idler bandwidth, emitted into the Gaussian collection modes. If the collected photons pass through spectral filters of narrow bandwidth, the effective brightness of the source is determined by the joint spectral density at the filter frequencies. Let us now consider the problem of maximizing this quantity, that is, finding the values of $\xi_p, \xi_s, \xi_i, \Phi$ that maximize $|\psi(\omega_s,\omega_i)|^2$ given the frequencies $\omega_p, \omega_s, \omega_i$ and crystal length L. From (16), it is apparent that maximization determines certain values $(A_+^{\max}, B_+^{\max}, \xi^{\max}, \Phi^{\max})$. The beam parameters ξ_p, ξ_s, ξ_i are then complicated functions of $(k_p, k_s, k_i, A_+^{\max}, B_+^{\max}, \xi^{\max}, \Phi^{\max})$ via relations (10)–(15). However, substantially more informative results can be obtained if the l^2 term in (16) is neglected. With $C \approx 0$ [approximation (18)], the function to be maximized is

$$\frac{1}{\sqrt{A_+ B_+}} \int_{-1}^{1} \frac{\sqrt{\xi}\exp(i\,\Phi l/2)}{1 - i\xi l}\,dl. \tag{22}$$

The two factors are independent and can be maximized separately. $A_+ B_+$ can be written as

$$A_+ B_+ = \left(1 - \frac{\Delta k}{k_p}\right)(1 + X_s r_s + X_i r_i)\left(1 + \frac{X_s}{r_s} + \frac{X_i}{r_i}\right),$$

where

$$X_j \equiv \frac{k_j}{k_p}\sqrt{\frac{1 + \Delta k/k_j}{1 - \Delta k/k_p}}, \tag{23}$$

$$r_j \equiv \frac{\xi_j}{\xi_p}\sqrt{\frac{1 - \Delta k/k_p}{1 + \Delta k/k_j}}. \tag{24}$$

The maximum of $(A_+ B_+)^{-1/2}$ occurs at $r_s = r_i = 1$. Invoking approximation (17) gives

$$\xi_s \approx \xi_i \approx \xi_p \approx \xi \tag{25}$$

and

$$\max \frac{1}{\sqrt{A_+ B_+}} \approx \frac{1}{2}. \tag{26}$$

The second factor in (22),

$$F(\xi, \Phi) \equiv \int_{-1}^{1} \frac{\sqrt{\xi}\exp(i\,\Phi l/2)}{1 - i\xi l}\,dl, \tag{27}$$

requires numerical evaluation and is plotted in Fig. 1. [Note that for $\xi \ll 1$, F is proportional to the usual phase-matching function $\text{sinc}(\Phi/2)$.] The maximum value of F is $2.06\ldots$ at $\xi = 2.84\ldots$, $\Phi = -(1.04\ldots)\pi$. This result, together with (26), yields the maximum spectral amplitude

$$\max_{\xi, \Phi} |\psi(\omega_s, \omega_i)| \approx 1.03 \sqrt{\frac{8\pi^2 \hbar \epsilon n_s n_i}{\varepsilon_0 n_p}} \frac{\chi_{\text{eff}}^{(2)}}{\lambda_s \lambda_i}\sqrt{N_p L}\,s(\omega_p), \tag{28}$$

which is obtained under the conditions

$$\xi_s \approx \xi_i \approx \xi_p \approx 2.84, \tag{29}$$

$$\Phi \approx -1.04\pi. \tag{30}$$

It should be noted that these are precisely the conditions which have long been known to maximize the efficiency
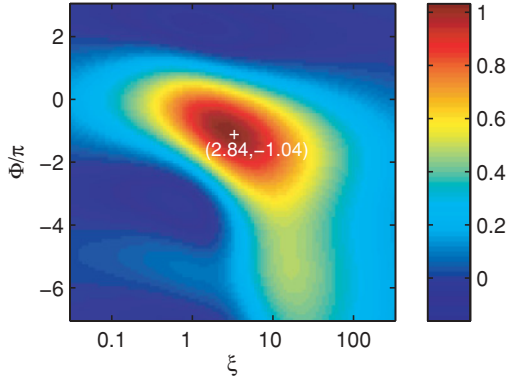
FIG. 1. (Color online) The spatial overlap factor $F(\xi, \Phi)$ defined in Eq. (27). The cross marks the location of the peak.

of sum-frequency generation and parametric amplification with Gaussian beams [19]. The spectral density $|\psi(\omega_s, \omega_i)|^2$ is proportional to the number of pump photons N_p and to the crystal length. [In contrast, for the case of collimated (plane wave) interaction, the spectral density would grow quadratically with the crystal length.] It may also be noted that, for all other factors being equal, short-wavelength sources are brighter than long-wavelength sources.

Because it may not always be possible to implement or verify condition (29) accurately, it is worth examining how sensitive the peak spectral density is to the focal parameters. Specifically, I compare $\max_\Phi |\psi|^2$, which is a function of (ξ_p, ξ_s, ξ_i), to the global maximum value $\max_{\xi, \Phi} |\psi|^2$. I constrain the parameter space by the condition $\xi_s = \xi_i$, which is not only optimal in regard to the spectral density but, as will be shown in later sections, is also optimal or near-optimal for other quantities of interest. Figure 2 shows the relative brightness $\max_\Phi |\psi|^2 / \max_{\xi, \Phi} |\psi|^2$ as a function of ξ_p and $\xi_s = \xi_i$. It can be seen that the regime of good focusing is rather broad: the waist size (and correspondingly, the angular divergence) must be made smaller or larger by roughly a factor of 5 to reduce the peak spectral density to half its maximum value. Over this range the optimal phase Φ (not shown) varies from $-\pi/2$ to $-3\pi/2$, meaning that the frequency of the peak shifts slightly with focusing. If the signal and idler focus
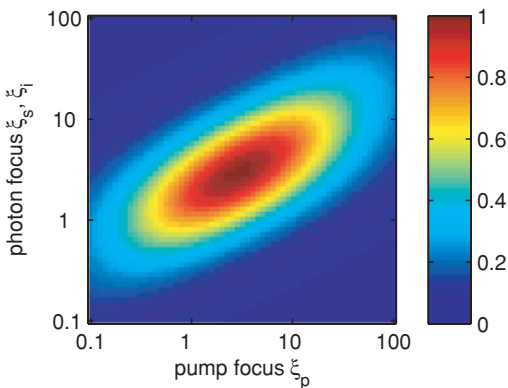

FIG. 2. (Color online) Peak joint spectral density, normalized to the global maximum, as a function of the pump and photon mode focus.

are fixed, the optimal pump focus is given by $\xi_p = \xi_s (= \xi_i)$. However, if the pump focus is fixed, the optimal signal and idler focus are given by $\xi_s = \xi_i \approx \sqrt{2.84\xi_p}$.

These results are robust to approximation: for the worst case defined in Sec. II, the "optimal" values given in (29) and (30) differ from the true optimal values by 5% and 10%, respectively, but, due to the broadness of ψ as a function of these parameters, they yield an amplitude that is within 1% of the actual maximum value.

IV. PHOTON BANDWIDTH WITH MONOCHROMATIC PUMPING

SPDC photons are sometimes employed in systems with limited optical bandwidth. In designing sources for such systems it is helpful to know how the photon bandwidths depend on the design parameters. One case of particular interest is when the pump bandwidth is chosen to maximize the spectral purity of the photons. That case will be addressed in Sec. VI. Another particularly interesting case is that of monochromatic pumping, which will be addressed now.

With a monochromatic pump, and under approximation (20), the spectral dependence of (16) arises primarily from the dispersion of the phase mismatch $\Phi = (\Delta k + mK)L$. The phase mismatch may be expanded as Taylor series in $\delta\omega_s$ and $\delta\omega_i$, the deviation of the signal and idler frequencies from their nominal values. Assumption (21) then gives

$$\Phi \approx \Phi_0 + \left(\frac{n_p'}{c}(\delta\omega_s + \delta\omega_i) - \frac{n_s'}{c}\delta\omega_s - \frac{n_i'}{c}\delta\omega_i \right) L, \quad (31)$$

where Φ_0 is the phase mismatch at the nominal frequencies. Monochromatic pumping constrains the frequencies to $\delta\omega_s = -\delta\omega_i$, yielding

$$\Phi \approx \Phi_0 + \frac{(n_s' - n_i')L}{c}\delta\omega_s. \quad (32)$$

The fact that Φ is (approximately) a linear function of ω_s means that the photon bandwidth $\Delta\omega_s (= \Delta\omega_i)$ can be expressed in terms of a dimensionless "phase mismatch bandwidth" $\Delta\Phi$, which is the width of $|\psi|^2$ when expressed as function of Φ.

Under approximation $C \approx 0$, $|\psi|^2$ is proportional to $|F(\xi, \Phi)|^2$. The full width at half-maximum (FWHM) of $|F(\xi, \Phi)|^2$ (see Fig. 1) was calculated numerically and is plotted as the solid line in Fig. 3. I find that the behavior of $\Delta\Phi$ in this case is captured well by the heuristic formula

$$\Delta\Phi \sim 2\pi \max(1, \xi/10), \quad (33)$$

shown as the dashed line. Combining (32) and (33) yields the photon bandwidths

$$\Delta\omega_s = \Delta\omega_i \sim \frac{2\pi c}{|n_s' - n_i'|} \max\left(\frac{1}{L}, \frac{1}{10b} \right) \quad (34)$$

where $b \equiv L/\xi$ is the aggregate confocal length of the modes (reducing to $k_p w_p^2$ when $\xi_s = \xi_i = \xi_p$). When focusing is weak to moderate ($\xi \lesssim 10$), the photon bandwidth is determined by the crystal length (the well-known $1/L$ dependence). But when the focusing is strong ($\xi \gtrsim 10$), the bandwidth is larger [20] and determined instead by the confocal length, going as $1/b$.
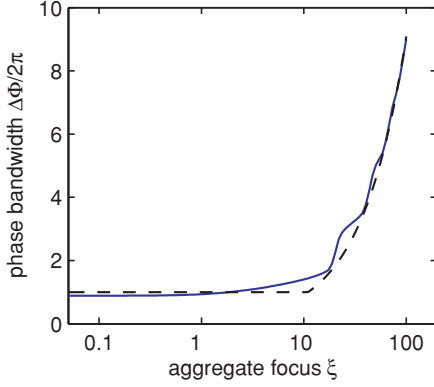
FIG. 3. (Color online) The normalized photon bandwidth as a function of focusing. The dashed line is the heuristic formula (33).

The reason that tightly focusing the pump increases the bandwidth can be understood as follows: At negative values of the phase mismatch (i.e., away from the nominal wavelengths), the photon spatial distribution in the far field takes the form of a ring [21]. With a collimated pump, a certain change in wavelength makes the ring radius larger than that of the collection modes, and photons of those wavelengths are not collected. But when the pump is tightly focused, the rings are spatially broadened and the photons partially overlap the collection mode [22]. The larger the spatial broadening, the larger the wavelength change must be for the photon distribution to lie outside the collection mode.

Owing to the approximation $C = 0$, the bandwidth plotted in Fig. 3 is not exact. For the reference source, the error in $\Delta\omega_s$ is $\leqslant 3\%$ for $\xi \leqslant 10$ and $\leqslant 10\%$ over the range $10 \leqslant \xi_p \leqslant 100$. For the worst typical case, the error is $\leqslant 3\%$ for $\xi \leqslant 1$ but increases to 10% at $\xi = 10$ and varies between 30% and 50% over the range $10 \leqslant \xi_p \leqslant 100$. Thus bandwidth predictions may not be highly accurate in the regime of focus-induced spectral broadening. Nevertheless, even in the worst case the approximate SPDC state $|\tilde{\psi}\rangle$ (calculated with $C = 0$) has a large overlap with the exact state $|\psi\rangle$ [calculated using (19)]: the fidelity $\langle\tilde{\psi}|\psi\rangle^2/\langle\tilde{\psi}|\tilde{\psi}\rangle\langle\psi|\psi\rangle$ is 0.999 at $\xi = 1$, 0.97 at $\xi = 10$, and 0.91 at $\xi = 100$. Also, the heuristic formula $\Delta\Phi \sim 2\pi\max(1, \xi/\xi_0)$ remains as accurate as shown in Fig. 3 for a suitably chosen value of ξ_0.

V. PAIR COLLECTION PROBABILITY

When SPDC photons are collected without spectral filtering, maximizing the pair collection probability

$$P_{si} = \int |\psi(\omega_s, \omega_i)|^2 d\omega_s d\omega_i \tag{35}$$

is usually more important than maximizing the peak spectral density. (In most experiments, P_{si} is proportional to the coincident photodetection rate, or the probability of detecting a pair of photons following any given pump pulse.) Under approximation (20), the dominant spectral dependence arises from $s(\omega_p)$ and Δk. The phase mismatch (31) may be written as

$$\Phi \approx \Phi_0 + \left(\frac{2n'_p - (n'_s + n'_i)}{2c}\delta\omega_p - \frac{n'_s - n'_i}{2c}\delta\omega_-\right)L, \tag{36}$$

where $\omega_- = \omega_s - \omega_i$. Then $d\omega_s d\omega_i = (d\omega_- d\omega_p)/2 = d\Phi d\omega_p\, c/(|n'_s - n'_i|L)$, giving

$$P_{si} = \frac{c}{|n'_s - n'_i|L}\int |\psi|^2\, d\omega_p d\Phi \tag{37}$$

$$= \frac{8\pi^2\hbar c\epsilon n_s n_i}{\varepsilon_0 n_p |n'_s - n'_i|}\left(\frac{\chi^{(2)}_{\text{eff}}}{\lambda_s\lambda_i}\right)^2 \frac{N_p}{A_+ B_+}\int \left| s(\omega_p) \right.$$

$$\left. \times \int_{-1}^{1} \frac{\sqrt{\xi}\exp([i\Phi l/2])}{1 - i\xi l - C\xi^2 l^2}\, dl \right|^2 d\omega_p d\Phi. \tag{38}$$

Under the approximation $C \approx 0$, the only place Φ appears is in the exponential function. Using $\int \exp[i\Phi(l - l')/2]\, d\Phi = 4\pi\delta(l - l')$ and $\int |s(\omega_p)|^2 d\omega_p = 1$, one obtains

$$P_{si} \approx \frac{32\pi^3\hbar c\epsilon n_s n_i}{\varepsilon_0 n_p |n'_s - n'_i|}\left(\frac{\chi^{(2)}_{\text{eff}}}{\lambda_s\lambda_i}\right)^2 \frac{N_p\xi}{A_+ B_+}\int_{-1}^{1}\frac{dl}{1 + \xi^2 l^2}, \tag{39}$$

which may be directly integrated to give

$$P_{si} \approx \frac{64\pi^3\hbar c\epsilon n_s n_i}{\varepsilon_0 n_p |n'_s - n'_i|}\left(\frac{\chi^{(2)}_{\text{eff}}}{\lambda_s\lambda_i}\right)^2 \frac{\arctan(\xi)}{A_+ B_+}N_p. \tag{40}$$

Formula (40), plotted as the dashed line in Fig. 4, suggests that the pair probability can only be optimized in an asymptotic sense—that there are no finite values of ξ_p, ξ_s, ξ_i that maximize P_{si}. In reality, the asymptotic behavior holds only as long as $\xi k_p/(4Lk_s k_i) \lesssim 0.1$. With very tight focusing or very short crystals, the approximation $C = 0$ breaks down, causing P_{si} to peak near its asymptotic value (solid lines in Fig. 4). In the worst typical case the pair probability error $|1 - \langle\tilde{\psi}|\psi\rangle/\langle\psi|\psi\rangle|$ is $\leqslant 4\%$ for $\xi \leqslant 1$, $\leqslant 13\%$ for $\xi \leqslant 10$, and $\leqslant 20\%$ for $\xi \leqslant 100$. For the reference source described above, the pair probability error is $\leqslant 1.5\%$ for $\xi \leqslant 100$. In any case, P_{si} evidently has an upper bound

$$P_{si} \leqslant \frac{8\pi^4\hbar c\epsilon n_s n_i}{\varepsilon_0 n_p |n'_s - n'_i|}\left(\frac{\chi^{(2)}_{\text{eff}}}{\lambda_s\lambda_i}\right)^2 N_p \tag{41}$$

that cannot be exceeded, no matter how long the crystal. (This somewhat surprising result will be discussed in Sec. VIII.) For
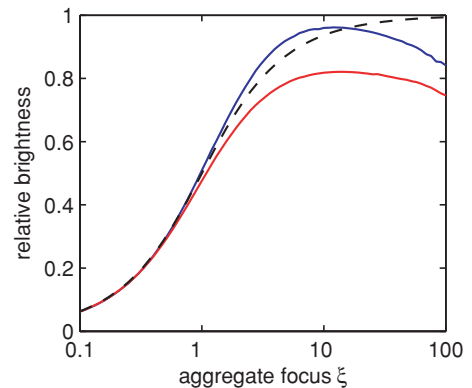

FIG. 4. (Color online) Dependence of the pair collection probability on the aggregate focus. The dashed line is Eq. (40) normalized by its asymptotic maximum. The solid lines are calculated using "worst case" values for the parameter C [see the discussion surrounding Eq. (19)] and normalized by the same factor.
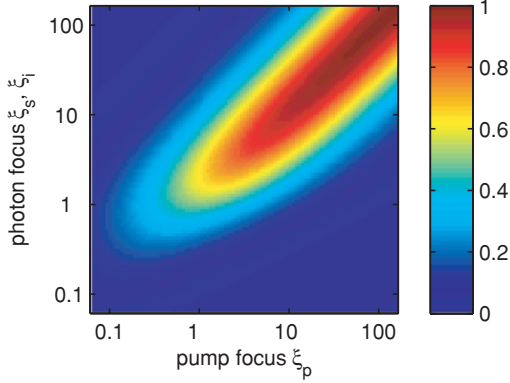
FIG. 5. (Color online) Dependence of the pair collection probability on the focus of the pump and photon modes.
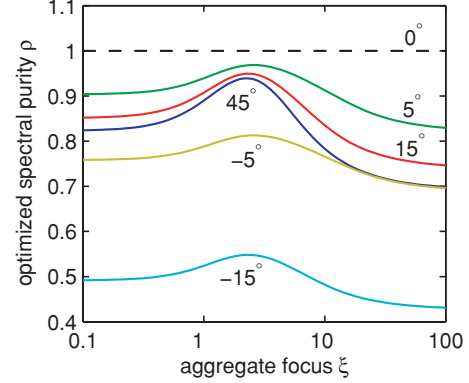

FIG. 6. (Color online) Dependence of the spectral purity of the collected photons on the mode focus. The numbers accompanying each line are the group velocity angle θ defined in Eq. (44). Solutions for $\theta \geqslant 45°$ mirror those for $\theta \leqslant 45°$.

type-II SPDC sources made of PPKTP or periodically poled lithium niobate (PPLN), Eq. (41) predicts that brightnesses exceeding 10^{-9} collected pairs per pump photon should be achievable—roughly an order of magnitude brighter than the brightest existing sources.

The dependence of P_{si} on ξ_{p} and $\xi_{\mathrm{s}} = \xi_{\mathrm{i}}$ is shown in Fig. 5. If the signal and idler focus are fixed, the optimal pump focus is given by $\xi_{\mathrm{p}} = \xi_{\mathrm{s}}(= \xi_{\mathrm{i}})$. If instead ξ_{p} is fixed, the optimal value of ξ_{s} is nearly equal to ξ_{p} for $\xi_{\mathrm{p}} \gtrsim 10$ and slightly larger than ξ_{p} for $\xi_{\mathrm{p}} \lesssim 10$.

VI. SPECTRAL PURITY

A number of applications of SPDC photons, including the generation of multiphoton entangled states for quantum computing [23–26], involve interference between photons from separate (and nominally identical) SPDC sources. The success of such applications depends not only on the efficiency of SPDC photon production, but also on the degree of mutual coherence of photons from independent sources [27,28]. This coherence, which is directly related to the interference visibility, is given by the single-photon purity

$$\rho = \frac{\sum_j \sigma_j^2}{\left(\sum_j \sigma_j\right)^2}, \tag{42}$$

where

$$\psi(\omega_{\mathrm{s}}, \omega_{\mathrm{i}}) = \sum_j \sqrt{\sigma_j} u_j(\omega_{\mathrm{s}}) v_j(\omega_{\mathrm{i}}) \tag{43}$$

is the Schmidt decomposition [29] of the collected biphoton state. The single-photon purity is inversely related to the degree of entanglement between the signal and idler frequencies, with $\rho = 1$ corresponding to no spectral entanglement. (Note that any spatial entanglement present in the emitted state is discarded upon postselecting photon pairs that couple into the Gaussian collection modes.)

It is natural to ask whether the parameters that yield high source brightness also yield high spectral purity. Under approximations (20) and (21), the frequency-dependent part of $\psi(\omega_{\mathrm{s}}, \omega_{\mathrm{i}})$ is $s(\omega_{\mathrm{p}}) F(\xi, \Phi)$. Since the purity depends only on the shape of $\psi(\omega_{\mathrm{s}}, \omega_{\mathrm{i}})$, and not on its location or extent within the $(\omega_{\mathrm{s}}, \omega_{\mathrm{i}})$ plane, ω_{s} and ω_{i} may be replaced with

the dimensionless variables $\omega_{\mathrm{s}}/\Omega$ and $\omega_{\mathrm{i}}/\Omega$, where $\Omega \equiv c/(n_{\mathrm{s}}' - n_{\mathrm{i}}')L$. Given a particular functional form for the pump spectrum, the purity may then be computed as a function of $(\xi, \theta, \Delta\omega_{\mathrm{p}}/\Omega)$ where $\Delta\omega$ is the pump bandwidth and

$$\tan\theta = \frac{n_{\mathrm{s}}' - n_{\mathrm{p}}'}{n_{\mathrm{p}}' - n_{\mathrm{i}}'} \tag{44}$$

is the slope, in the $(\omega_{\mathrm{s}}, \omega_{\mathrm{i}})$ plane, of the line characterized by $\Phi = 0$. Note that since ξ is the only relevant focusing parameter, we are free to set $\xi_{\mathrm{s}} \approx \xi_{\mathrm{i}} \approx \xi_{\mathrm{p}}$ to maximize the brightness at a given $(\xi, \theta, \Delta\omega_{\mathrm{p}}/\Omega)$. Also, note that the brightness is independent of the pump bandwidth when approximation (21) is valid.

The spectral purity obtainable with a Gaussian pump was determined by computing $s(\omega_{\mathrm{p}}) F(\xi, \Phi)$ over a grid of sufficient extent and resolution in the $(\omega_{\mathrm{s}}/\Omega, \omega_{\mathrm{i}}/\Omega)$ plane for various parameter values $(\xi, \theta, \Delta\omega_{\mathrm{p}}/\Omega)$. For each set of parameter values, singular value decomposition was applied to the matrix of computed values to determine $\{\sigma_j\}$ and ρ. Numerical optimization was then used to determine the value of $\Delta\omega_{\mathrm{p}}/\Omega$ that maximizes ρ at each (ξ, θ). In Fig. 6 these optimized values of ρ are plotted as a function of $\xi (= \xi_{\mathrm{p}})$ for several different values of θ. For $\theta = 45°$, the peak purity is 0.94 and occurs at $\xi = 2.2$. As θ decreases to $0°$, ρ asymptotically increases to 1 for all values of ξ, although the optimal pump bandwidth becomes infinite in this limit. Below $0°$, ρ drops rapidly. Solutions for $\theta \geqslant 45°$ mirror those for $\theta \leqslant 45°$, with the signal and idler exchanging roles.

These results can be understood as follows. The purity is directly related to the factorability of $\psi(\omega_{\mathrm{s}}, \omega_{\mathrm{i}}) \propto s(\omega_{\mathrm{p}}) F(\xi, \Phi)$ into separate functions of ω_{s} and ω_{i}. When the pump function $s(\omega_{\mathrm{p}})$ is Gaussian, complete factorability can be achieved if and only if the phase-matching function $F(\xi, \Phi)$ is also Gaussian with orientation $0 \leqslant \theta \leqslant \pi/2$ [5]. But $F(\xi, \Phi)$ is not Gaussian: for $\xi \ll 1$ it is a sinc function, which has oscillating side lobes, while for $\xi \gg 1$ it has large skew. In both these regimes, the purity is reduced. $F(\xi, \Phi)$ is most nearly Gaussian for $\xi \sim 2$, which becomes the regime of greatest purity.

By comparing Figs. 2 and 4, one sees that in the regime of peak purity ($\xi \sim 2$) the spectral intensity is close to its peak value and the total collection probability is more than 70% of its asymptotic maximum (41). Thus, high spectral purity ($\geqslant 94\%$) can be obtained with focusing conditions that also yield relatively high brightness, provided $0 \leqslant \theta \leqslant 90°$ (which amounts to the requirement that n'_p lie between n'_s and n'_i).

An explicit evaluation of the accuracy of these results in view of approximation (18) was not performed. However, it may be noted that the results of this section are based on a decomposition of an approximate state which, as discussed at the end of Sec. IV, has a high degree of overlap with the actual state.

VII. SINGLE-PHOTON COLLECTION AND HERALDING RATIO

In some applications of SPDC, the detection of a photon in the signal mode is used to indicate the (probable) presence of a photon in the idler mode. (Although the photons are always emitted in pairs, conditions generally allow one photon to be emitted into a spatial mode defined by the collection optics while its partner is emitted into a noncollected spatial mode.) In such applications it is desirable to have a high *heralding ratio* $\eta_s \equiv P_{si}/P_s$, where P_s is the probability that a photon is emitted into the signal collection mode, regardless of the mode its partner is in. Since the probability of collecting both photons cannot exceed the probability of collecting one of the photons, the heralding ratio can be at most unity. In applications that treat signal and idler photons symmetrically, the quantity $\eta_{si} \equiv P_{si}/\sqrt{P_s P_i}$ is often the metric of choice. In this work η_s will be called the signal heralding ratio and η_{si} will be called the symmetric heralding ratio.

To obtain the signal collection probability P_s, the joint collection probability must be summed over a complete set of spatial modes for the idler photon. The Laguerre-Gauss modes

$$\mathbf{E}^{(n,l)}(\mathbf{r}; \omega) = \frac{\mathbf{e}}{\sqrt{\pi/2}} \left(\frac{w_i}{q_i}\right)^{l+1} \left(\frac{q_i^*}{q_i}\right)^n L_n^l \left(\frac{2w_i^2 \rho^2}{|q_i|^2}\right)$$
$$\times \exp\left(-\frac{\rho^2}{q_i} + i k_i z + i l \phi\right) \quad (45)$$

form such a set, where L_n^l is the (n,l) associated Laguerre polynomial, $\rho = \sqrt{x^2 + y^2}$, and $\tan \phi = x/y$. The fundamental mode with $n = l = 0$ is just the Gaussian mode introduced in Sec. II. Since the pump and signal mode are azimuthally symmetric, the spatial overlap vanishes unless the idler mode is also azimuthally symmetric ($l = 0$). Thus the spatial overlap involving the nth idler mode is

$$\mathcal{O}_n = \frac{\sqrt{\epsilon}\, \chi_{\text{eff}}^{(2)}}{(\pi/2)^{3/2}} \int_{-L/2}^{L/2} \int_0^\infty \frac{w_p w_s w_i}{q_p q_s^* q_i^*} \left(\frac{q_i}{q_i^*}\right)^n L_n\left(\frac{2w_i^2 \rho^2}{|q_i|^2}\right)$$
$$\times \exp\left[-\rho^2 \left(\frac{1}{q_p} + \frac{1}{q_s^*} + \frac{1}{q_i^*}\right) + i(\Delta k + mK)z\right]$$
$$\times 2\pi \rho \, d\rho \, dz. \quad (46)$$

With the Laguerre polynomial expansion formula $L_n(x) = \sum_{j=0}^n (-1)^j \frac{n!}{(n-j)! j! j!} x^j$ and a bit of work, one can obtain

$$\mathcal{O}_n = \sqrt{\frac{8\epsilon}{\pi}} \chi_{\text{eff}}^{(2)} w_p w_s w_i \int_{-L/2}^{L/2} \frac{\exp[i(\Delta k + mK)z]}{q_s^* q_i^* + q_p q_i^* + q_p q_s^*}$$
$$\times \left(\frac{q_s^* q_i + q_p q_i - q_p q_s^*}{q_s^* q_i^* + q_p q_i^* + q_p q_s^*}\right)^n dz. \quad (47)$$

Applying definitions (10)–(14) and making the approximation $C \approx 0$ yields

$$\mathcal{O}_n \approx \chi_{\text{eff}}^{(2)} \sqrt{\frac{2\epsilon}{\pi}} \frac{k_s k_i}{k_p} L \sqrt{\frac{\xi_s \xi_i}{\xi_p}} \int_{-1}^1 \frac{\exp(i\Phi l/2)}{A_+ - il B_+ \xi_s \xi_i / \xi_p}$$
$$\times \left(\frac{A_- + il B_- \xi_s \xi_i / \xi_p}{A_+ - il B_+ \xi_s \xi_i / \xi_p}\right)^n dl. \quad (48)$$

In analogy with formulas (35) and (5), the signal photon probability may be written as $P_s = \int \sum_{n=0}^\infty |\psi_n(\omega_s, \omega_i)|^2 d\omega_s d\omega_i$, where $\psi_n = \sqrt{2\pi^2 \hbar N_p / \epsilon_0 \lambda_p \lambda_s \lambda_i} s(\omega_p) \mathcal{O}_n(\omega_s, \omega_i)$. Following the approach taken in Sec. V, we have

$$P_s \approx \frac{8\pi^2 \hbar c \epsilon n_s n_i N_p}{\epsilon_0 n_p |n'_s - n'_i|} \left(\frac{\chi_{\text{eff}}^{(2)}}{\lambda_s \lambda_i}\right)^2 \frac{\xi_s \xi_i}{\xi_p}$$
$$\times \sum_{n=0}^\infty \int \left|\int_{-1}^1 \frac{\exp(i\Phi l/2)}{A_+ - il B_+ \xi_s \xi_i / \xi_p}\right.$$
$$\times \left.\left(\frac{A_- + il B_- \xi_s \xi_i / \xi_p}{A_+ - il B_+ \xi_s \xi_i / \xi_p}\right)^n dl\right|^2 d\Phi \quad (49)$$

$$= \frac{32\pi^3 \hbar c \epsilon n_s n_i N_p}{\epsilon_0 n_p |n'_s - n'_i|} \left(\frac{\chi_{\text{eff}}^{(2)}}{\lambda_s \lambda_i}\right)^2 \xi_s \int_{-1}^1 \frac{dl}{A_s^2 + (B_s \xi_s)^2 l^2}, \quad (50)$$

where

$$A_s = 2\sqrt{\left(1 + \frac{k_s}{k_p} \frac{\xi_s}{\xi_p}\right) \frac{k_i}{k_p}}, \quad (51)$$

$$B_s = 2\left(1 - \frac{\Delta k}{k_p}\right) \sqrt{\left(1 + \frac{k_s + \Delta k}{k_p - \Delta k} \frac{\xi_p}{\xi_s}\right) \frac{k_i + \Delta k}{k_p - \Delta k}}. \quad (52)$$

Integration yields the signal collection probability

$$P_s \approx \frac{64\pi^3 \hbar c \epsilon n_s n_i}{\epsilon_0 n_p |n'_s - n'_i|} \left(\frac{\chi_{\text{eff}}^{(2)}}{\lambda_s \lambda_i}\right)^2 \frac{\arctan\left(\frac{B_s}{A_s} \xi_s\right)}{A_s B_s} N_p. \quad (53)$$

The corresponding formula for the idler probability P_i can be obtained by interchanging the labels s and i everywhere. Equation (53) is very similar to Eq. (40) and holds under essentially the same conditions. Like P_{si}, the signal probability P_s is (to first approximation) an asymptotically increasing function of focal parameters, with an upper bound

$$P_s \leqslant \frac{32\pi^4 \hbar c \epsilon n_s n_i}{3\epsilon_0 n_p |n'_s - n'_i|} \left(\frac{\chi_{\text{eff}}^{(2)}}{\lambda_s \lambda_i}\right)^2 N_p. \quad (54)$$

Also like P_{si}, P_s is locally maximized by taking $\xi_s \approx \xi_p$ (see Fig. 5); however, P_s varies more slowly with ξ_s and ξ_p than P_{si} (Fig. 7). The fact that P_s is broader than P_{si} means that collection of the signal in a nonoptimal Gaussian mode projects the idler onto a mode that does not couple well to a Gaussian mode of any size (i.e., a mode that is not Gaussian). Note also
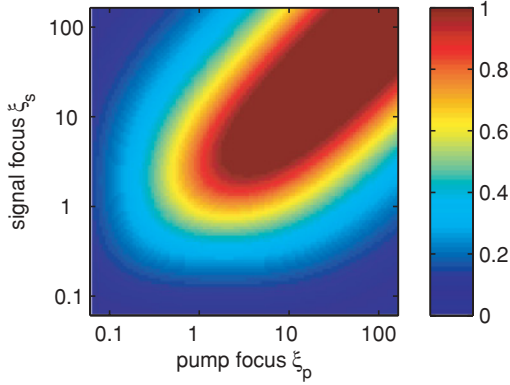
FIG. 7. (Color online) Dependence of the signal collection probability on the focus of the pump and signal modes for near-degenerate SPDC ($k_s \approx k_i \approx k_p/2$).

that (53) is independent of ξ_i as it should be (the parameters of the idler collection mode should be irrelevant when one does not care whether the idler is collected).

If one takes $\xi_s = \xi_i = \xi_p$, which locally maximizes both P_{si} and P_s, the signal heralding ratio reduces to the simple expression

$$\eta_s = \frac{k_i}{k_p}\left(\frac{k_s}{k_p} + 1\right). \tag{55}$$

An analogous expression exists for η_i. These expressions give $\eta_s = \eta_i = 0.75$ for near-degenerate SPDC (for which $k_s \approx k_i \approx k_p/2$) and values less than 0.75 for the nondegenerate case. However, higher heralding ratios are possible with different focusing conditions. The optimal source configuration with regard to both heralding and brightness is not a single set of parameter values, but a curve in parameter space that has the

property that η_s (or η_{si}, if that is of interest) cannot be increased without decreasing P_{si}, and vice versa. Numerical methods were used to find the values (ξ_s, ξ_i, ξ_p) that maximize either η_s or η_{si} at 50 values of P_{si} covering the range from 0 to max P_{si}. The resulting points are plotted versus ξ_p in Fig. 8 for the case $k_s \approx k_i \approx k_p/2$. Figure 8 shows that it is possible to achieve very high heralding ratios, but only with a substantial reduction in brightness: a factor of at least 4 to achieve $\eta_s \geqslant 0.95$ and a factor of at least 10 to achieve $\eta_{si} \geqslant 0.95$. That is, there is a trade-off between brightness and the heralding ratio, which is somewhat worse for symmetric heralding than asymmetric heralding. Both η_s and η_{si} approach unity in the limit that the pump is collimated ($\xi_p \to 0$). In this limit the best trade-off between P_{si} and η_{si} is achieved with $\xi_s = \xi_i \gg \xi_p$, while the best trade-off between P_{si} and η_s is achieved with $\xi_i \approx 3\xi_s \approx 3\xi_p$. The trade-offs between P_{si} and η_s or η_{si} are found to be slightly worse in the nondegenerate case than the near-degenerate case.

VIII. DISCUSSION

Perhaps the most significant finding of this study is that there exist focusing conditions ($\xi_p, \xi_s, \xi_i \sim 2.5$) that simultaneously bring the brightness, heralding ratio, and spectral purity to substantial fractions of their maximal values. Whenever n'_p lies between n'_s and n'_i, a spectral purity of at least 0.94 can be obtained with at least 74% of the maximum achievable brightness, while the heralding ratio is at least 0.75 (for near-degenerate SPDC). Maximum brightness can be achieved with tighter focusing at the cost of reducing the spectral purity (to 0.7 at worst). The worst trade-off is between brightness and the heralding ratio: focusing conditions that yield a symmetric (asymmetric) heralding ratio of 0.95 or better reduce the
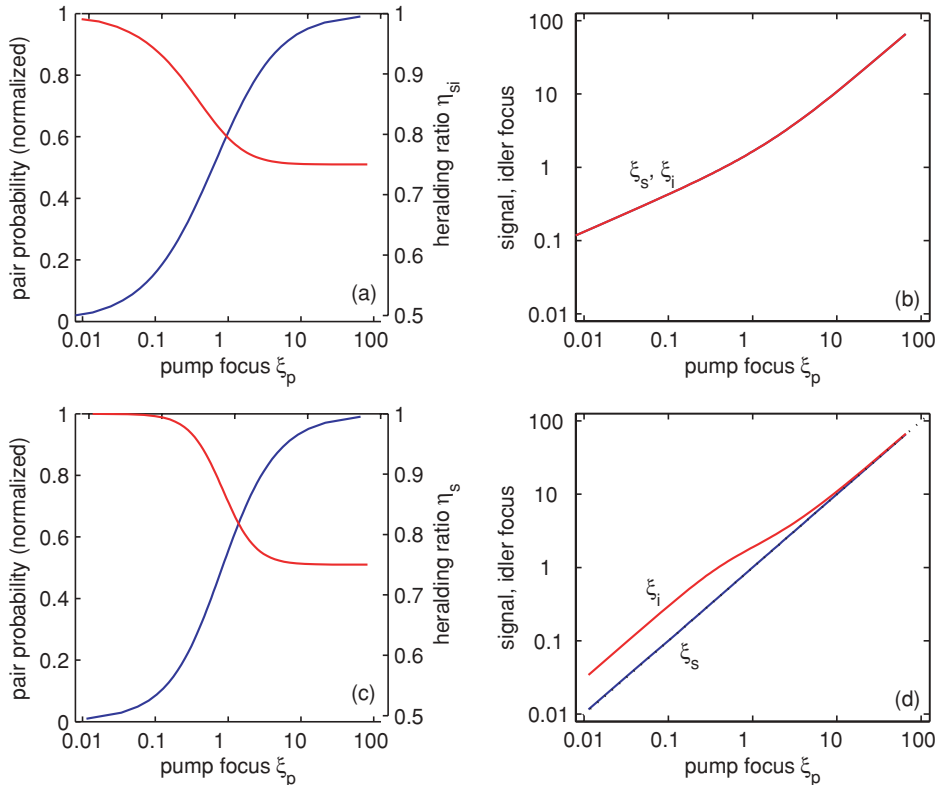

FIG. 8. (Color online) (a) and (b) Simultaneous optimization of the total collection probability P_{si} and the symmetric heralding ratio η_{si}. (c) and (d) Simultaneous optimization of P_{si} and the signal heralding ratio η_s. Panels (b) and (d) plot the focal parameters that yield the optimal curves shown in (a) and (c), respectively. In (a) and (c) the collection probability goes with the left axis and the heralding ratio goes with the right axis.

brightness to 10% (25%) of its maximal value; however, the spectral purity remains 0.84 or better.

Another notable finding of this study is that many important properties of the collected SPDC state are essentially scale invariant. To the extent that the parameter C [see (14)] is negligibly small, the joint collection probability, heralding ratios, and spectral purity are determined by the dimensionless ratios $L/k_j w_j^2$ and $\Delta\omega_p L/c$. Changing the crystal length has no effect on these three quantities if the pump duration and confocal ranges are also scaled by the same factor. In the end, the crystal length merely sets the bandwidth of the system, with longer crystals yielding (or requiring) smaller bandwidths. The idea that a longer crystal does not yield a brighter source is perhaps surprising, since longer crystals yield higher SPDC efficiencies when the pump is collimated or weakly focused. Why this is not so for *optimally focused* sources may be understood by noting that, although a shorter crystal has a shorter interaction length (which decreases the spatial mode overlap), it also allows the modes to be focused more tightly (which increases the mode overlap). Of course, this argument does not hold for arbitrarily short crystals; at some point, the focusing becomes so strong and the bandwidths become so large that the paraxial approximation implicit in (7), as well as approximations such as (20), break down. At the other extreme, very long crystals may also show worse than expected performance due to the challenge of manufacturing very long crystals of high quality.

Some of the results obtained here appear to agree with prior works, while others appear to differ from prior works. The focusing condition $\xi_s = \xi_i = \xi_p = 2.84$ which maximizes the joint spectral density of SPDC is the same as that found by Boyd and Kleinman for maximizing second-harmonic generation (SHG) [19]. This makes sense, since SHG with a monochromatic Gaussian input beam produces a monochromatic Gaussian second-harmonic field; optimization of SHG then amounts to finding the parameters of the Gaussian modes that maximize the spatial overlap, which is precisely what was done in Sec. III. More recently, Ljunggren and Tengner [14] have performed numerical studies yielding the optimizing conditions $2\xi_p = 1.7$, $2\xi_s = 2\xi_i = 2.3$, and the prediction that the optimized joint probability goes as $\sqrt{L}$ (rather than being independent of L as claimed here). These discrepancies may be due to two key differences in approach: In [14], optimal focusing conditions are obtained for $\Phi = 0$, whereas here and in [19] the condition $\Phi = -1.04\pi$ is found to yield a slightly higher spectral density. Additionally, [14] employs a plane-wave approach in which the diffraction of the pump mode is effectively ignored; this approximation is also made in [13], [11], and [15]. In the present study the pump is treated as a diffracting paraxial beam. Experiments to date are insufficient to resolve these differences as they cover a limited range of crystal lengths and focal parameters, and are complicated by poor repeatability (changing the focus of a beam, or replacing a crystal with one of different length, generally necessitates realignment).

The results of this study are intended to be useful for designing and predicting the approximate performance of a promising class of SPDC sources. A number of points should be kept in mind, however. Firstly, all the results presented here apply to the *collected* part of the biphoton state; many features of the emitted SPDC light are lost or substantially altered when the state is projected onto the Gaussian collection modes. Secondly, while care was taken to confirm the general viability of the approximations employed, it is not difficult to envision sources that would violate the assumptions of this analysis and exhibit quantitatively or qualitatively different performance. In particular, results obtained here may not be reliable for very short sources ($L \lesssim 1$ mm), sources with very short poling periods ($\Lambda \lesssim 5\,\mu$m), and/or sources employing quasi-phase-matching of order $m > 1$. Thirdly, certain physical details deemed inconsequential—such as the vector diffraction of the Gaussian beams, the optical anisotropy of nonlinear crystals, and the proper normalization of electromagnetic modes quantized in a dielectric—were simply ignored. Fourthly, a limitation of this study is that it does not apply to angle-tuned sources in which beam walk-off plays a role. However, since walk-off decreases spatial overlap, it is not clear that such sources could achieve better overall performance than the collinear sources considered here. Finally, of all the results obtained here, only those in Sec. III are potentially applicable to frequency-degenerate type-I sources. The quadratic relationship between frequency and phase mismatch in these sources substantially complicates analysis; however, the possibility that these sources might have different scaling laws makes them potentially worth a comparable study.

IX. SUMMARY

In summary, I have presented here a theoretical study of SPDC addressing multiple properties of the emitted photons that are important in various applications. Analysis was restricted to the promising class of SPDC sources involving focused, collinear Gaussian modes for the pump field and collected photons. Analytical and numerical calculations yielded approximate predictions for the peak spectral density, photon bandwidths, absolute pair collection probability, heralding ratio, and spectral purity. A scaling law was found which shows most of these properties to be ultimately independent of crystal length. It was also found that such sources can simultaneously exhibit high brightness (predicted 10^{-9} pairs per pump photon), high spectral purity ($\geqslant 0.94$), and a moderately high heralding ratio ($\gtrsim 0.75$) when the confocal ranges of the modes are on the order of half the crystal length. Higher heralding ratios can be achieved, at the cost of significantly reduced brightness, by focusing the modes less tightly. The results of this study are applicable to "typical" SPDC sources, excluding sources of very short length, very short poling period, or very large bandwidth. Frequency-degenerate type-I sources, which often do not satisfy these criteria, may be amenable to a similar kind of study.

[1] A. Politi, J. C. F. Matthews, M. G. Thompson, and J. L. O'Brien, IEEE J. Sel. Top. Quantum Electron. **15**, 1673 (2009).

[2] M. Peev *et al.*, New J. Phys. **11**, 075001 (2009).

[3] F. Wong, J. Shapiro, and T. Kim, Laser Physics **16**, 1517 (2006).

[4] A. Fedrizzi, T. Herbst, A. Poppe, T. Jennewein, and A. Zeilinger, Opt. Express **15**, 15377 (2007).

[5] W. P. Grice, A. B. U'Ren, and I. A. Walmsley, Phys. Rev. A **64**, 063815 (2001).

[6] A. B. U'Ren, Y. Jeronimo-Moreno, and H. Garcia-Gracia, Phys. Rev. A **75**, 023810 (2007).

[7] P. J. Mosley, J. S. Lundeen, B. J. Smith, and I. A. Walmsley, J. Mod. Opt. **56**, 179 (2009).

[8] T. S. Humble and W. P. Grice, Phys. Rev. A **75**, 022307 (2007).

[9] C. Kurtsiefer, M. Oberparleiter, and H. Weinfurter, Phys. Rev. A **64**, 023802 (2001).

[10] F. Bovino, P. Varisco, A. Colla, G. Castagnoli, G. Di Giuseppe, and A. Sergienko, Opt. Commun. **227**, 343 (2003).

[11] A. Dragan, Phys. Rev. A **70**, 053814 (2004).

[12] R. Andrews, E. Pike, and S. Sarkar, Opt. Express **12**, 3264 (2004).

[13] S. Castelletto, I. Degiovanni, G. Furno, V. Schettini, A. Migdall, and M. Ware, IEEE Trans. Instrum. Meas. **54**, 890 (2005).

[14] D. Ljunggren and M. Tengner, Phys. Rev. A **72**, 062301 (2005).

[15] A. Ling, A. Lamas-Linares, and C. Kurtsiefer, Phys. Rev. A **77**, 043834 (2008).

[16] P. Kolenderski, W. Wasilewski, and K. Banaszek, Phys. Rev. A **80**, 013811 (2009).

[17] C. K. Hong and L. Mandel, Phys. Rev. A **31**, 2409 (1985).

[18] P. Evans, J. Schaake, R. Bennink, T. Humble, and W. Grice (in preparation).

[19] G. D. Boyd and D. A. Kleinman, J. Appl. Phys. **39**, 3597 (1968).

[20] S. Carrasco, A. V. Sergienko, B. E. A. Saleh, M. C. Teich, J. P. Torres, and L. Torner, Phys. Rev. A **73**, 063802 (2006).

[21] P. G. Kwiat, K. Mattle, H. Weinfurter, A. Zeilinger, A. V. Sergienko, and Y. H. Shih, Phys. Rev. Lett. **75**, 4337 (1995).

[22] Z. Zhao, K. A. Meyer, W. B. Whitten, R. W. Shaw, R. S. Bennink, and W. P. Grice, Phys. Rev. A **77**, 063828 (2008).

[23] C.-Y. Lu, X.-Q. Zhou, O. Guhne, W.-B. Gao, J. Zhang, Z.-S. Yuan, A. Goebel, T. Yang, and J.-W. Pan, Nature Phys. **3**, 91 (2007).

[24] M. Radmark, M. Zukowski, and M. Bourennane, Phys. Rev. Lett. **103**, 150501 (2009).

[25] W. Wieczorek, R. Krischek, N. Kiesel, P. Michelberger, G. Toth, and H. Weinfurter, Phys. Rev. Lett. **103**, 020504 (2009).

[26] R. Prevedel, G. Cronenberg, M. S. Tame, M. Paternostro, P. Walther, M. S. Kim, and A. Zeilinger, Phys. Rev. Lett. **103**, 020503 (2009).

[27] A. U'Ren, E. Mukamel, K. Banaszek, and I. Walmsley, Philos. Trans. R. Soc. London A **361**, 1493 (2003).

[28] T. S. Humble and W. P. Grice, Phys. Rev. A **77**, 022312 (2008).

[29] C. K. Law, I. A. Walmsley, and J. H. Eberly, Phys. Rev. Lett. **84**, 5304 (2000).